Mapping Cell Morphology to a Standard Coordinate System for Analyzing Dynamic Cell Signaling

Shiqiu Yu
Lyda Hill Department of Bioinformatics
UT Southwestern Medical Center
Dallas, Texas, USA
Shiqiu.Yu2@UTSouthwestern.edu

Gaudenz Danuser
Institute of Human Biology (IHB)
Roche Pharma Research & Early Development
F. Hoffmann-La Roche Ltd
Basel, Switzerland
gaudenz.danuser@roche.com

Felix Y. Zhou
Lyda Hill Department of Bioinformatics
UT Southwestern Medical Center
Dallas, Texas, USA
felix.zhou@UTSouthwestern.edu

Abstract

Cell shape influences spatial signal distribution and serves as a key non-genetic regulatory mechanism of cell behavior. A global shape change, from a round to a flat shape, amplify concentration everywhere in the cell volume. Meanwhile, high-curvature protrusions can diffusion trap, locally amplifying, or excluding concentrations. Unfortunately, cell shape is heterogeneous, varying significantly between cells, and can change dramatically in the same cell over time. A key analytical challenge is measuring the local molecular signal everywhere in the cell in a manner that enables comparative analyses of signal distribution across cells and over time. Here, we developed a framework to bijectively map 2D cell shapes into a 2D disk. Using a cell shape dataset (Cellpose), we validated our method enables complete sampling of intracellular signal everywhere for diverse cell shapes. We apply our mapping to investigate correlations between the cell interior and boundary Cdc42 signal distribution with the cell edge dynamics of a migrating neutrophil-like cell during chemotaxis.

1 Introduction

Deciphering the linkage between molecular signals and cell shape is fundamental to a more mechanistic understanding of how molecular processes govern cell behavior. Cytoskeletal controlling Rac1 and Cdc42 molecules localize to the cell edge and induce the local formation of lamellipodia and ruffles[1], and filopodia[2], three different types of cell surface protrusions. In turn, these protrusions influence the local molecular concentration of signaling molecules which can amplify or suppress signaling cascades controlling behavior e.g. proliferation. In melanoma cells, lamellipodia helped sequester tumor suppressor proteins that promote cell survival[3], enabling them to survive chemotherapy drug treatment.

Quantifying an interaction between morphology and signal requires measuring and comparing the intracellular signal pattern across shapes. However, the large diversity in cell shape presents two fundamental challenges: (i) how to partition shape into 'windows' to sample the local signal, and (ii) how to establish correspondence between the windows of different cells or the same cell at different timepoints. Both tasks are trivial for regular geometries like the circle, that support equipartitioning

The 3rd Workshop on Imageomics: Discovering Biological Knowledge from Images Using AI

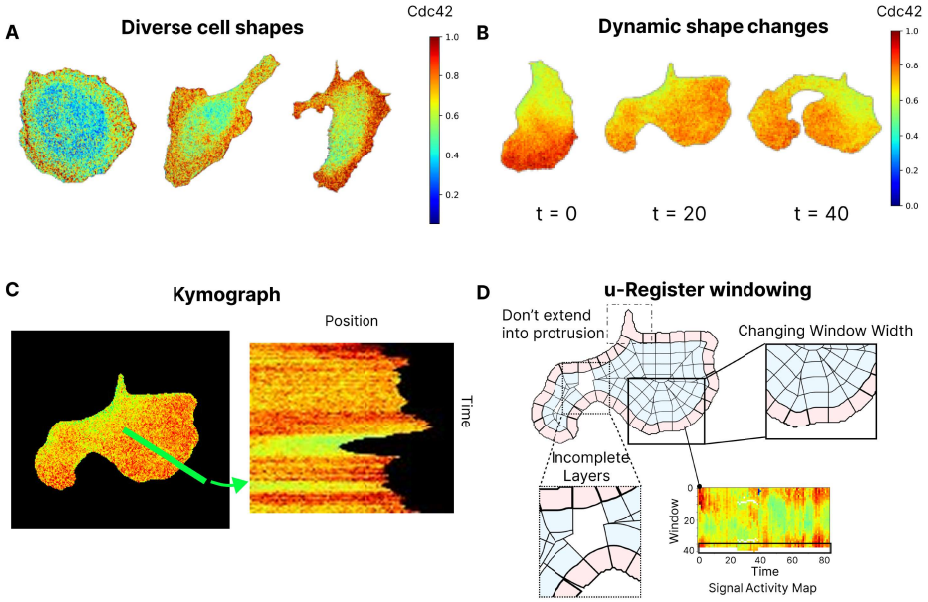

Figure 1: **Cell shape variation challenges regular sampling of intracellular signal**. (A) Diverse shapes. (B) Shape at different timepoints. (C) Kymograph of signal intensity over time sampled along the green line. (D) u-Register[5–7] edge-based windowing of cell in (C).

for (i), and requires only rotational registration to align signal distributions for (ii). Unfortunately, cell shapes are non-convex, often elongated and branched, and can have complex boundaries decorated by high-curvature protrusions,(Fig.1A,B).

Here, we developed a general solution using differential geometry techniques to map 2D cell shapes and their intracellular signals into a 2D disk domain. We can then (i) window the disk and use the mapping to also window the cell, and (ii) use the disk geometry to establish spatiotemporal correspondence and perform consistent, complete and regular windowing of dynamic cell shapes. Crucially, the existence of a disk mapping is guaranteed by the uniformization theorem[4] for any cell shape that is simple i.e. has no topological holes. In practice, we can satisfy this condition by morphological operations such as binary infilling of inaccurate cell segmentations.

2 Related Works

Various approaches have been established to sample timeseries of signals. Linescans or kymographs are a space–time plot of the signal profile across time along a manually-specified line-of-interest (Fig.1C). Kymographs provide a direct readout of local signal activity but suffers key limitations: subregion selection is subject to human bias, does not establish temporal correspondences, and the subregion activity may not represent the behavior in other cell regions. Nonrigid image registration[8] register cell shapes to a single reference shape. However, concave features, notably necks, cellular protrusions, and branches, that are only a few pixels wide pose ambiguity in the learning of deformation fields. The current state-of-the-art is edge-based windowing methods[5, 9, 7]. These first equipartition the boundary, and extends the partition guided by the gradient of a distance transform inwards to the cell interior. In this manner, a cell is windowed in 'layers'. u-Register[5–7], the most influential software for edge-based windowing of cells, additionally models the window edges as 'springs' to maximize the regularity of individual windows - rectangular-shaped, equal area and aspect ratio, (Fig.1D). However, u-Register windows cannot tile into narrow, high-curvature protrusions, and degenerate - shrinking in covered area and breaking regularity when mapping the cell interior and along the medial-axis skeleton of the shape. Moreover, for concave shapes, windows of the cell interior in the same layer are spatially disconnected. This leads to windows with no measured signal, and sparse signal activity maps - a kymograph representation of window intensity across time,[6] and complicates their use for cross-correlation[6, 10] and causality analyses[11] between the activity of two signals and between a signal and morphology, namely, edge protrusion velocity.

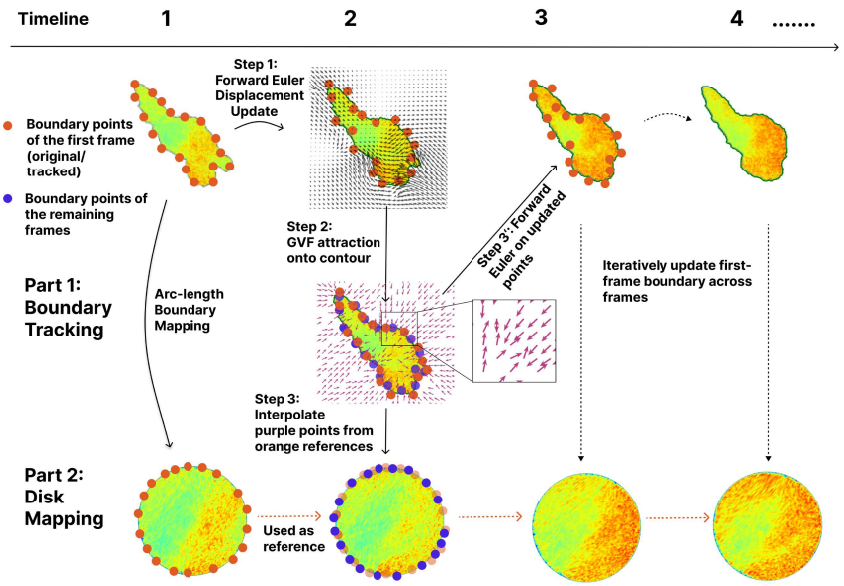

Figure 2: Overview of the u-Unwrap framework to sample intracellular signal in dynamic cell shapes.

3 Methods

Our framework consists of two components: (i) multi-frame boundary tracking to maintain consistent sampling of the same local boundary region across time, and (ii) remapping of irregular cell shape into a disk domain to establish spatiotemporal correspondence of the interior area for uniform and temporally-consistent sampling of intracellular signals, (Fig.2). Mathematical details are described in Appendix A.

(i) Multi-frame Boundary Tracking. We propagate the N shape boundary points of the first timepoint frame-to-frame. To propagate from time t to $t+1$, we first displace the points using the displacement field found by applying symmetric forces demons registration[12] on the binary cell segmentation images. Then, we correct for residual registration errors, including misalignment of cell protrusions. We iteratively propagate the demons displaced points until convergence along a gradient vector field (GVF) whose attractor is the segmented cell shape at $t+1$. Finally, we equally resample N equidistant points using the boundary of the cell shape $t+1$ formed by the final propagated point locations. This latter redistribution step is crucial. It serves the same role as the line tension regularization in u-Register in maintaining complete sampling of the boundary across all timepoints, and preventing concentration of points to local areas of high edge movement.

(ii) Mapping a single 2D cell shape into a 2D disk. For a single cell shape, we map the cell boundary points to the boundary of the 2D disk, preserving the relative arc-length of adjacent cell boundary points. We then map the cell interior points by solving the Laplace equation (Appendix A) using the 2D disk coordinates of the cell boundary as the fixed boundary conditions. The result is a conformal map which preserves local angles, but severely shrinks high-curvature boundary regions in the disk, particularly narrow branches and cell protrusions. To enable proportionate sampling of the cell shape, we update the disk points to uniformize the induced area-distortion of the initial conformal map. The final equiareal map establishes coordinate correspondence between the (u, v) disk and (x, y) cell space. Signal intensities are mapped to the disk by interpolation at the corresponding (x, y) coordinates. For video, we map the first frame boundary points to the disk boundary by preserving arc length as for single shapes. For each subsequent frame, we use the propagated points of the first frame to find the mapping of the cell shape boundary at time t in the disk parameterization of the first frame. We then map the cell interior at time t as for single shapes, now using the found disk coordinates of the cell boundary as the fixed boundary conditions in the Laplace equation, and relaxing the area distortion in the resulting conformal map. This mapping establishes correspondence of the cell interior across time.

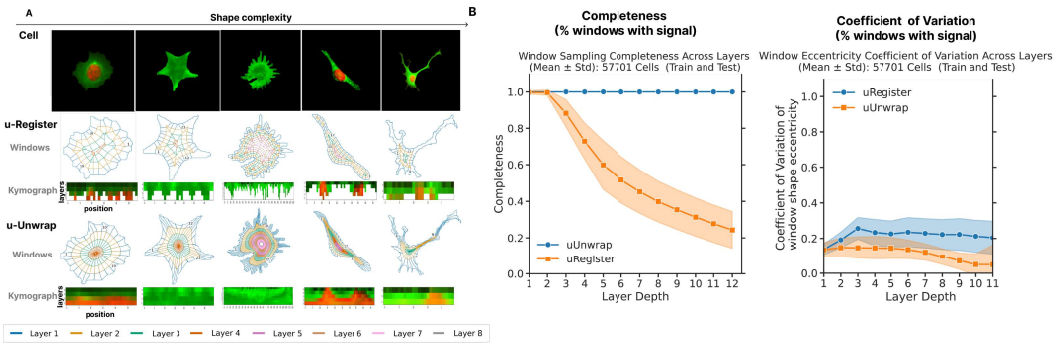

Figure 3: u-Unwrap vs u-Register windowing of cell shapes in the Cellpose[13] dataset.

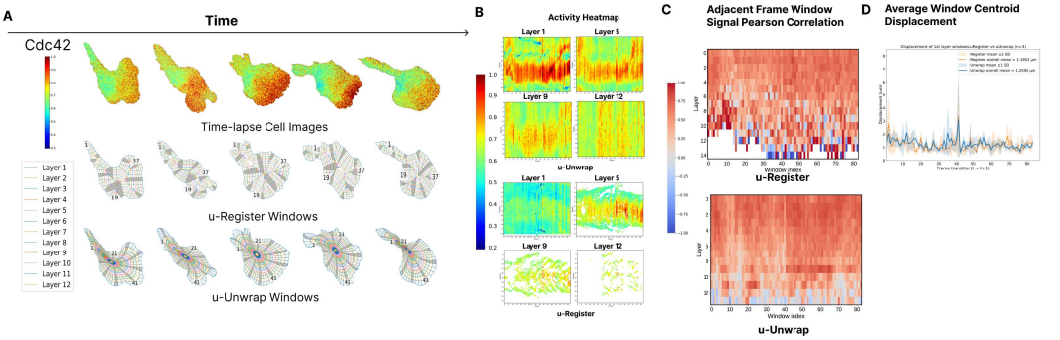

Figure 4: u-Unwrap vs u-Register windowing of a migrating neutrophil-like cell

Windowing the cell using the disk parameterization. To window the cell, we partition the disk into equal-sized radial quadrants by radius (for depth) and arc length (for boundary). Then we remap the disk windows back to the cell space.

4 Results

We performed three experiments to verify the improved windowing performance of our proposed framework, u-Unwrap with state-of-the-art u-Register for both single and dynamic cell shapes.

4.1 u-Unwrap enables complete mapping of heterogeneous single cell shapes

We derived a shape complexity score to select five representative cells in the Cellpose [13] dataset to validate that u-Unwrap completely windows the interior area across diverse cell shapes. For each cell, we applied both u-Register and u-Unwrap. u-Register parameters were manually tuned to achieve the best possible windowing with maximal coverage of the cell area, including slender extensions and narrow tails. We then applied u-Unwrap with matched parameters to obtain the same number of boundary windows and depth layers. We could then directly compare both methods for windowing completeness, defined as the fraction of windows that sample signal. Visually, u-Register produced regular windows in regions with regular geometry, but failed to partition small protrusive spikes (Fig.3A). u-Register windows also had varying widths within the same layer and across layers, particularly in regions corresponding to convex and concave cell boundary regions. In contrast, u-Unwrap consistently partitioned these challenging regions into relatively uniform windows within each layer. Crucially, u-Unwrap windows sample signal in every window (100% completeness), whereas u-Register window completeness decreased rapidly at increasing interior depth, (Fig.3B).To assess the variation in window eccentricity, we calculated the coefficient of variation for each layer of windows across both methods.(Fig.3B) The u-unwrap method consistently shows lower values after the first layer, indicating that the window shapes change more consistently across layers.

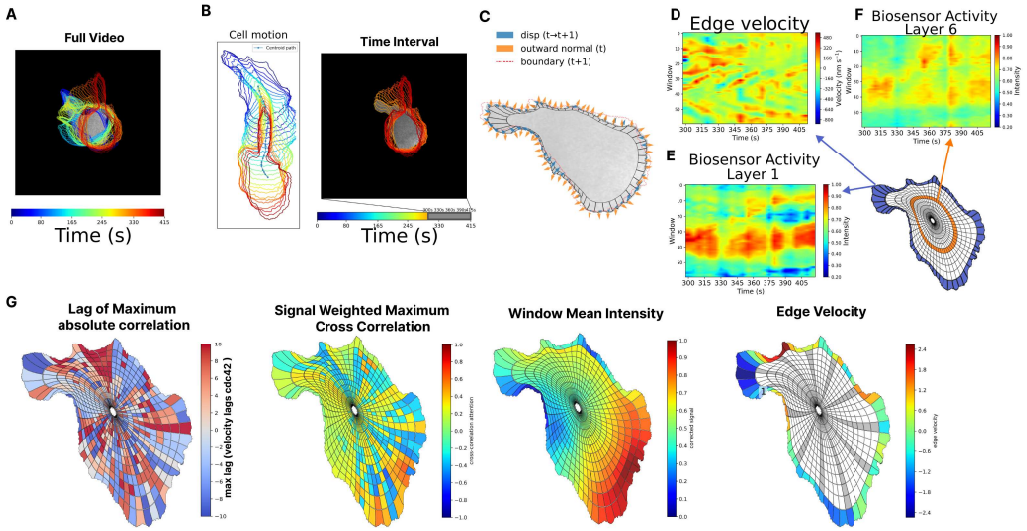

Figure 5: Cross-correlation analysis between biosensor activity and edge velocity inside the cell

4.2 u-Unwrap enables more consistent sampling of intracellular single in dynamic cell shapes

We next compared the ability of u-Unwrap and u-Register to window and sample the activity of Cdc42 in three neutrophil-like cells during chemotaxis whose shape undergoes pronounced changes[10] (Fig.4). We follow the same parameter-selection strategy as used for single shapes, targeting ≈60 windows along the cell boundary, each with a depth of 10 pixels (1.6μm) into the cell as used previously[10]. Visually, both methods generated temporally stable windows (Fig.4A). However, the u-Register Cdc42 activity maps severely undersample signal in windows from interior layers (Fig.4B). To quantitatively assess temporal tracking consistency, we computed (i) the Pearson correlation of window-averaged Cdc42 signal between consecutive timepoints for each depth layer (Fig.4C); and (ii) the mean centroid displacement of a window between consecutive timepoints (Fig.4D). Whereas, u-Unwrap maintained both consistently high correlations and low window displacements across all timepoints, u-Register exhibited two peaks of significantly elevated window displacement, indicating mistracked windows, and increased sensitivity to large shape changes.The calculated displacements show similar magnitudes for both methods. However, the cross-correlation between consecutive frames in u-Unwrap exhibits more consistent values across all layers. Tracking is challenging in the long, slanted region for both methods; however, u-Register is prone to completely missing these areas, whereas u-Unwrap can still sample data there (see Appendix S3). These regions may contain significant signals that reflect cell movements.

4.3 u-Unwrap enables cross-correlation analysis of intracellular signals beyond the cell edge

Using the ability of u-Unwrap to now completely sample the signal within a cell, we sought to investigate how the signal dynamics in the cell interior, far from the cell edge, influences edge velocity during migration. As the neutrophil-like cell exhibits pronounced shape changes (Fig.5A), which also suggests a dynamic underlying signal-morphology correlation structure, we only performed u-Unwrap analysis for a shorter time interval to assess proof-of-principle, (Fig.5B). For each u-Unwrap window we computed its mean edge velocity by (i) mapping the disk points corresponding to the cell edge back onto the cell boundary at all timepoints; (ii) computing the displacement of each point between consecutive frames; (iii) computing for each point, the component of its displacement in the direction of the local outward-pointing edge normal vector; and (iv) computing the mean of the projected displacements, (Fig.5C). We then performed cross-correlation analysis of the Cdc42 signal activity in every window with the edge velocity of its angularly-corresponding window in layer 1 (Fig.5D-F). To visualize the results, for each window, we mapped the maximum correlation and its associated time lag back onto the cell, considering both positive and negative correlations and retaining the smaller lag to reduce potential spurious signal associations, (Fig.5G). This revealed local coordination between edge and interior windows evidenced by similar correlations and lags, and suggest Cdc42 organize in microdomains to effect local shape change and direct migration. We

further evaluated our method on a Rac1–RhoA dataset by performing cross-correlation analysis across all possible spatial window pairs (Appendix FigS4). This approach captures not only the peripheral but also the intracellular regions of the cells, allowing us to investigate long-range coupling between the two signals in motile cells. The analysis reveals both positive and negative correlations at long and short spatial distances in the dynamic coupling of RhoA and Rac1, which likely reflect mechanical long-range interactions and biochemical short-range interactions, respectively.

5 Conclusion

In this work, we introduced the u-Unwrap framework to completely sample intracellular signals within diverse cell shapes, and with improved temporal consistency. This paves the way for the development of downstream analyses to study the influence of intracellular signaling beyond the cell edge in coordinating cell behavior. A limitation of u-Unwrap is a more expensive runtime due to computing on dense mesh-based representations. Also, the disk mapping is only bijective for topologically simple cell shapes, those containing no holes. Our current equipartition windowing also does not account for salient intracellular structures like the nucleus. Future work will explore how to overcome these computational issues and develop alternative biology-driven disk partitioning schemes to enhance the specificity and interpretability of windows.

6 Code Availability

u-Unwrap is available from GitHub, https://github.com/DanuserLab/u-unwrap. u-Unwrap can run on CPU only on a standard laptop or desktop machine with 16GB RAM.

7 Acknowledgements

This project was funded by an NIH grant, grant ID:R35 GM136428 to Prof. Gaudenz Danuser. We thank Prof. Sean R. Collins for providing the migration videos of neutrophil-like cells. We thank Prof. Louis Hodgson for the Rac1-RhoA videos.

References

[1] Anne J Ridley, Hugh F Paterson, Caroline L Johnston, Dagmar Diekmann, and Alan Hall. The small gtp-binding protein rac regulates growth factor-induced membrane ruffling. *Cell*, 70(3): 401–410, 1992.

[2] Robert Kozma, Sohail Ahmed, Anthony Best, and Louis Lim. The ras-related protein cdc42hs and bradykinin promote formation of peripheral actin microspikes and filopodia in swiss 3t3 fibroblasts. *Molecular and cellular biology*, 15(4):1942–1952, 1995.

[3] Ashwathi S Mohan, Kevin M Dean, Tadamoto Isogai, Stacy Y Kasitinon, Vasanth S Murali, Philippe Roudot, Alex Groisman, Dana K Reed, Erik S Welf, Sangyoon J Han, et al. Enhanced dendritic actin network formation in extended lamellipodia drives proliferation in growth-challenged rac1p29s melanoma cells. *Developmental cell*, 49(3):444–460, 2019.

[4] Lars Valerian Ahlfors. *Lectures on quasiconformal mappings*, volume 38. American Mathematical Soc., 2006.

[5] Matthias Machacek and Gaudenz Danuser. Morphodynamic profiling of protrusion phenotypes. *Biophysical journal*, 90(4):1439–1452, 2006.

[6] Matthias Machacek, Louis Hodgson, Christopher Welch, Hunter Elliott, Olivier Pertz, Perihan Nalbant, Amy Abell, Gary L Johnson, Klaus M Hahn, and Gaudenz Danuser. Coordination of rho gtpase activities during cell protrusion. *Nature*, 461(7260):99–103, 2009.

[7] Hunter Elliott, Shann-Ching Chen, Kwonmoo Lee, Michelle C. Mendoza, Sebastien Besson, and Gaudenz Danuser. Manuscript documenting algorithms for cell boundary tracking and sampling window propagation implemented in u-register software, June 2025. URL `https://doi.org/10.5281/zenodo.15765708`.

[8] Xuexia Jiang, Tadamoto Isogai, Joseph Chi, and Gaudenz Danuser. Fine-grained, nonlinear registration of live cell movies reveals spatiotemporal organization of diffuse molecular processes. *PLOS Computational Biology*, 18(12):e1009667, 2022.

[9] Masataka Yamao, Honda Naoki, Katsuyuki Kunida, Kazuhiro Aoki, Michiyuki Matsuda, and Shin Ishii. Distinct predictive performance of rac1 and cdc42 in cell migration. *Scientific reports*, 5 (1):17527, 2015.

[10] Hee Won Yang, Sean R Collins, and Tobias Meyer. Locally excitable cdc42 signals steer cells during chemotaxis. *Nature cell biology*, 18(2):191–201, 2016.

[11] Jungsik Noh, Tadamoto Isogai, Joseph Chi, Kushal Bhatt, and Gaudenz Danuser. Granger-causal inference of the lamellipodial actin regulator hierarchy by live cell imaging without perturbation. *Cell systems*, 13(6):471–487, 2022.

[12] Tom Vercauteren, Xavier Pennec, Aymeric Perchant, Nicholas Ayache, et al. Diffeomorphic demons using itk's finite difference solver hierarchy. *The Insight Journal*, 1:1–8, 2007.

[13] Carsen Stringer, Tim Wang, Michalis Michaelos, and Marius Pachitariu. Cellpose: a generalist algorithm for cellular segmentation. *Nature Methods*, 18(1):100–106, 2021. doi: 10.1038/s41592-020-01018-x.

[14] Chenyang Xu and Jerry L Prince. Gradient vector flow: A new external force for snakes. In *Proceedings of IEEE computer society conference on computer vision and pattern recognition*, pages 66–71. IEEE, 1997.

[15] Mario Botsch and Leif Kobbelt. A remeshing approach to multiresolution modeling. In *Proceedings of the 2004 Eurographics/ACM SIGGRAPH symposium on Geometry processing*, pages 185–192, 2004.

[16] Felix Y Zhou, Andrew Weems, Gabriel M Gihana, Bingying Chen, Bo-Jui Chang, Meghan Driscoll, and Gaudenz Danuser. Surface-guided computing to analyze subcellular morphology and membrane-associated signals in 3d. *bioRxiv*, 2023.

[17] Guangyu Zou, Jiaxi Hu, Xianfeng Gu, and Jing Hua. Authalic parameterization of general surfaces using lie advection. *IEEE Transactions on Visualization and Computer Graphics*, 17(12): 2005–2014, 2011.

[18] Felix Y. Zhou. Spot (shape, appearance, motion phenotype observation tool), 2023. URL `https://github.com/fyz11/SPOT`.

[19] Leland McInnes, John Healy, and James Melville. Umap: Uniform manifold approximation and projection for dimension reduction. *arXiv preprint arXiv:1802.03426*, 2018.

A Mathematical details of the u-Unwrap framework

A.1 Boundary Tracking

To enable temporally-consistent disk mapping of cell shapes across time points of a video, we performed (1) rigid-body registration to remove global translation and rotation of shape, then (2) propagated the cell boundary points of the first frame across subsequent frames.

1. Global registration to remove translation and rotation between consecutive frames.

We perform registration to remove first any global translation and rotation of the whole cell shape. As the neutrophil-like cell undergoes pronounced changes, instead of using the shape of a single timepoint as reference, we perform this registration sequentially across timepoints, switching the timepoint used as reference every nth frame. For the neutrophil-like cell, we empirically determined N=5 frames.

Algorithm 1: Sequential rigid registration

Input: $\{I_0, I_1, ..., I_t\}, n$; (video frames at time, I_t)
Output: $\{I_0^r, I_1^r, ..., I_t^r\}$; (registered video frames at time, I_t^r)
$I_{ref} \leftarrow I_0$; (initialize $t = 0$ as reference)
for $t = 0 : T$ **do**
  if $t \mod n = 0$ ***and*** $t > 0$ **then**
    $I_{ref} \leftarrow I_{t-1}^r$; (Set last registered timepoint as reference)
  end
  $register(I_{ref}, I_t)$; (Register to reference)
end

2. Propagating the first frame cell boundary points across time

We propagate the boundary points of the binary cell segmentation at time t found by Marching Cubes onto the boundary of the binary segmentation at time t sequentially in time. Between consecutive timepoints, t and $t + 1$, we do

(i) Symmetric forces demons non-rigid registration. We perform pairwise registration between consecutive binary cell segmentations, I_t, I_{t+1} to obtain the displacement field, $d_{t,t+1}(x, y) = (\Delta x(x, y), \Delta y(x, y))$ mapping points at time, t at position (x, y) to their position at $t + 1$:

$$d_{1,2} \leftarrow \text{register } I_2 \text{ to } I_1, \qquad d_{2,3} \leftarrow \text{register } I_3 \text{ to } I_2),$$

(ii) Forward Euler propagation of boundary using demons displacement fields

Let $B_t = \{(x_i^t, y_i^t)\}_{i=1}^N$ and N denote the number of boundary points at time $t = 0$. We find the positions of individual points at time $t + 1$ by a forward Euler update using $d_{t,t+1}(x, y) = (\Delta x(x, y), \Delta y(x, y))$:

$$x_i^{t+1} = x_i^t + \Delta x(x_i^t, y_i^t), \qquad y_i^{t+1} = y_i^t + \Delta y(x_i^t, y_i^t),$$

(iii) Gradient vector field (GVF) refinement to ensure propagated points map to the next timepoint cell boundary

To ensure the demons displacement field propagated points, $\{(x_i^{t+1}, y_i^{(s)})\}_{i=1}^N$ from (ii) lie on the actual boundary of the binary cell segmentation at time $t + 1$, we refine the positions using the constructed gradient vector flow (GVF)[14], $\mathbf{g}_{t+1}(x, y)$ whose attractor is the boundary of the binary cell segmentation at time $t + 1$. To refine, we stably deform the demons displacement field boundary using the active contours model[14] with a step size of 1 pixel for 100 iterations to ensure convergence.

(iv) Reparameterization of GVF refined boundary

We parameterize the GVF-refined boundary using B-splines $(X(u), Y(u))$ to resample N equidistant boundary points as the boundary at time $t + 1$, $B_{t+1} = \{(x_i^{t+1}, y^t t + 1_i)\}_{i=1}^N$, where N is the same

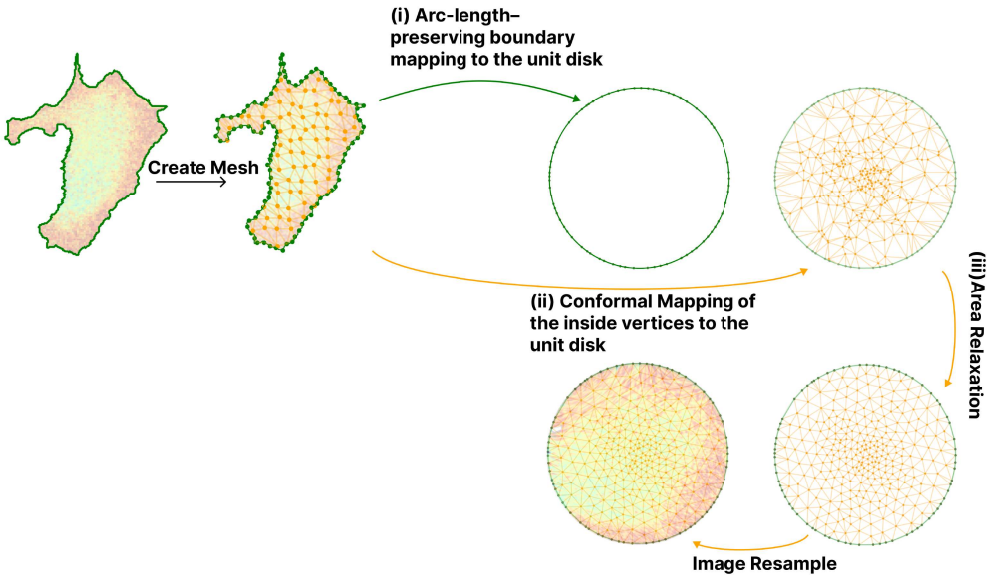

Fig. S1: u-Unwrap mapping of a single cell shape into a disk using conformal mapping and area distortion relaxation.

number of boundary points in the first frame. This reparameterization is necessary to maintain uniform tracking of the cell boundary over time and prevent aggregation of points to boundary regions that experience the largest displacements.

Combined, steps (i-iv) allow stable, long-term tracking of local boundary protrusion and retraction, even for large changes in cell shape.

A.2 Mapping 2D cell shapes into a 2D disk

The mapping of 2D cell shape is performed on triangle meshes. We construct from the binary cell segmentation image, $B \in \mathbb{R}^{H\times W}$, whose pixel value at location,(x, y) is 1 if it is part of the cell, and 0, otherwise, a triangular mesh whereby vertices are the pixels belonging to the cell, and forming the triangle face connectivity by subdividing the grid connectivity among pixels. To allow for optimal area-distortion relaxation later, the mesh should be isotropic, with triangles that are near-equilateral. To obtain an isotropic mesh we remesh the initial mesh formed from grid connectivity using the isotropic incremental remeshing algorithm[15]. This isotropic mesh cell representation is used to perform the mapping which involves three steps: (i) mapping the cell boundary points to the disk boundary; (ii) mapping the cell interior points to the disk interior using a conformal map; and (iii) area distortion relaxation to obtain the final equiareal disk parameterization. The process is illustrated in Fig.S1.

In the following, we denote the vertices of the isotropic mesh as $V_{cell} = \{v_1^{cell}, v_2^{cell}, \ldots, v_N^{cell}\}$, $v_i^{cell} = (x_i, y_i) \in \mathbb{R}^2$ and its corresponding coordinates on the unit disk, $V_{disk} = \{v_1^{disk}, v_2^{disk}, \ldots, v_N^{disk}\}$, $v_i^{disk} = (u_i, v_i) \in \mathbb{R}^2 : u_i^2 + v_i^2 \leq 1$. We denote the ordered loop of boundary vertices of the cell mesh, $B_{cell} = \{v_{b_1}^{cell}, v_{b_2}^{cell}, \ldots, v_{b_n}^{cell}\} \subset V_{cell}$, and the other interior vertices by $I_{cell} = V_{cell} \setminus B_{cell}$. To computationally implement all algorithmic steps we adapted functions from the u-Unwrap3D Python package [16] for 2D images.

A.2.1 Mapping a single cell shape

(i) Mapping the boundary points by arc-length preservation

We map the cell boundary vertices, B_{cell} onto the boundary of the unit disk, whilst preserving the relative arc length between neighbor vertices. Specifically, we map each boundary point $v_{b_k}^{cell}$ as

$$(u_{b_k}, v_{b_k}) = \big(\cos\theta_{b_k},\ \sin\theta_{b_k}\big), \quad \text{where} \quad \theta_{b_k} = \frac{2\pi s_{b_k}}{S}$$

$s_{b_k} = \sum_{k=2}^{k=k} ||v_{b_k}^{cell} - v_{b_{k-1}}^{cell}||$ is the cumulative arc length along the boundary from $v_{b_1}^{cell}$ up to the point, $v_{b_k}^{cell}$, and S is the total perimeter length of the cell boundary.

(ii) Mapping the interior points using a conformal map

Given the boundary coordinate correspondence $\{v_{b_k}^{cell} \mapsto (u_{b_k}, v_{b_k})\}$, the conformal map, $\varphi : V \to D$ of cell interior points, I_{cell}, onto the unit disk, $D = \{z \in \mathbb{R}^2 \mid \|z\| \leq 1\}$ is computed by solving the discrete Laplace equation,

$$L\varphi = 0$$

using the established boundary coordinate correspondence from (i) as Dirichlet boundary conditions. L is the cotangent Laplacian matrix constructed from the mesh connectivity, and φ is the desired corresponding $\{(u_i, v_i)\}$ coordinates.

(iii) Area distortion relaxation to obtain an equiareal disk parameterization

Denoting the triangle faces of the cell mesh as $\{T_j\}$, the local area distortion factor, λ_j of triangle j in the conformal disk parameterization $\varphi(\Omega)$ is defined as

$$\lambda_j = \frac{\text{Area}(\varphi(T_j))/\sum_j \text{Area}(\varphi(T_j))}{\text{Area}(T_j)/\sum_j \text{Area}(T_j)}$$

To reduce local area distortion we need to iteratively displace vertex positions within the disk. However, minimizing the defined λ_j is numerically unstable because of its dependence on the initial cell mesh[16]. Instead, noting that given an isotropic cell mesh, the triangle area in the conformal disk parameterization already reflects the local area distortion, we follow u-Unwrap3D[16] and use the proxy area distortion factor, λ_j^{proxy} given by

$$\lambda_j^{proxy} = \frac{\text{median}\left(\text{Area}(\varphi(T_j))/\sum_j \text{Area}(\varphi(T_j))\right)}{\text{Area}(\varphi(T_j))/\sum_j \text{Area}(\varphi(T_j))}$$

Minimizing this proxy area distortion factor whose numerator is constant-valued is equivalent to uniformizing the triangle areas in the disk parameterization.

To displace vertices to diffuse λ_j^{proxy} in the disk, we use the Lie advection framework for area-preserving parameterization[17], which first solves a Laplace-style equation to compute a smooth field of λ_j^{proxy}, to perform Forward Euler gradient descent steps on the cell interior disk vertices,

$$\varphi^{(t+1)}(v_i) = \varphi^{(t)}(v_i) + \epsilon\, \nabla\lambda_j^{proxy}, \qquad v_i \in I_{cell}$$

where the $\nabla\lambda_j^{proxy}$ is the per-vertex vectors obtained by averaging the original per-face vectors onto vertices, and ϵ is a small step size. Delaunay flips between iterations to ensure bijectivity. Boundary vertices remain fixed on the boundary of the unit disk. We perform 500 iterations to ensure optimal area distortion relaxation is reached for all shapes in the Cellpose dataset.

A.2.2 Mapping a temporal sequence of cell shapes

To map a temporal sequence of cell shapes obtained from video data onto the disk, the procedure is similar to a single shape. The primary difference is the cell boundary is tracked to ensure consistent mapping of the cell boundary at times $t > 0$ into the same disk parameterization of time $t = 0$.

Mapping the boundary at time $t > 0$ onto the disk boundary of $t = 0$

Given the disk parameterization of the boundary at the first timepoint, $t = 0$, the propagated boundary coordinates of the first timepoint, at time t, $\{\tilde{x}_i\}$, and the boundary points of the binary cell segmentation at time t, $\{x_i\}$, we find the disk coordinates of $\{x_i\}$ using a local two-nearest-neighbor (2-NN) scheme. For each x_i, we find its nearest propagated point $\tilde{x}_j$, and its successor, $\tilde{x}_{j+1}$ in the boundary. Then, using their corresponding disk coordinates, (u_j, v_j) and (u_{j+1}, v_{j+1}), with angles $\theta_j = \arctan 2(v_j, u_j)$ and $\theta_{j+1} = \arctan 2(v_{j+1}, u_{j+1})$, we compute the distances, $d_j = \|x_i - \tilde{x}_j\|$, $d_{j+1} = \|x_i - \tilde{x}_{j+1}\|$ to assign inverse-distance weights, $w_j = \frac{1}{d_j}$, $w_{j+1} = \frac{1}{d_{j+1}}$, respectively. The interpolated angular position on the disk parameterization is given by the weighted average, $\theta_i(x_i) = \frac{w_j\theta_j + w_{j+1}\theta_{j+1}}{w_j + w_{j+1}}$, and $(u_i, v_i) = (\cos\theta_i, \sin\theta_i)$.

Mapping the cell interior at time t

We find the conformal map of the cell interior points by solving the discrete Laplace equation for a single cell shape using now the (u_i, v_i) coordinates of the boundary at times $t > 0$. Subsequently, we perform area distortion relaxation in the same manner as for a single cell shape.

B Computation of a shape complexity score for shapes in the Cellpose dataset

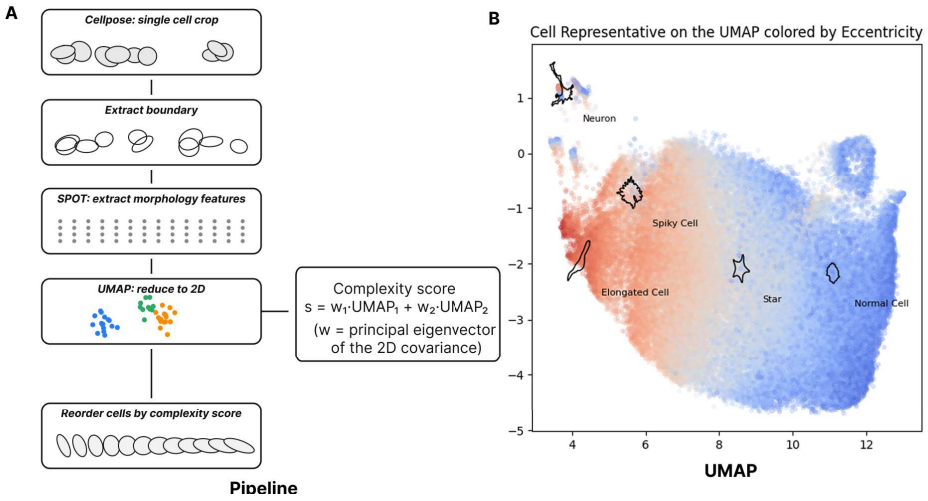

Fig. S2: Shape Complexity Score Calculation

We derived a score of shape complexity for shapes in the Cellpose[13] training dataset as illustrated in Fig.S2A as follows:

1. For each shape, compute a shape feature vector using the SPOT package[18]
2. Apply UMAP[19] to project shapes by their SPOT shape feature vector into two dimensions, $(umap_1, umap_2)$
3. Find the principal eigenvector through the UMAP 2D coordinates, $(umap_1, umap_2)$ by eigenvalue decomposition
4. Compute the complexity score as the projection of each shape's UMAP coordinate onto the UMAP principal eigenvector.

We manually selected five cells spanning the complexity score range to represent the morphological diversity in the dataset, and possessed distinct morphological features e.g. elongated, branching, that pose different challenges for a windowing method, (Fig.S2B).

C Neutrophil-like cells windowing visualization comparison

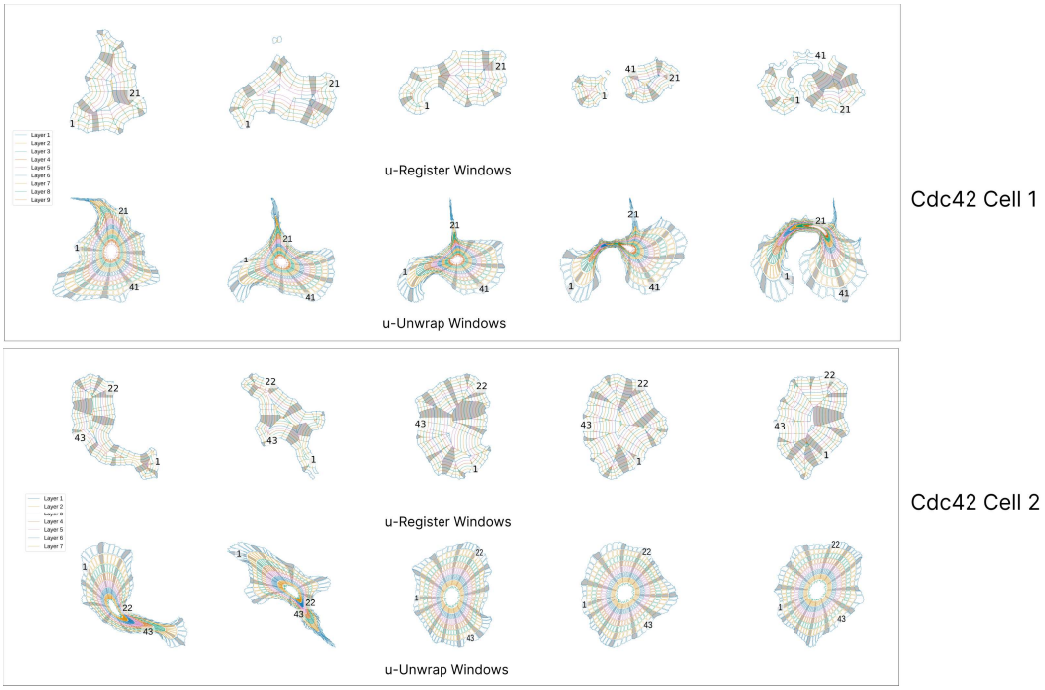

Fig. S3: Comparison of windowing displays between the two methods.

D Long range analysis of coupling signals

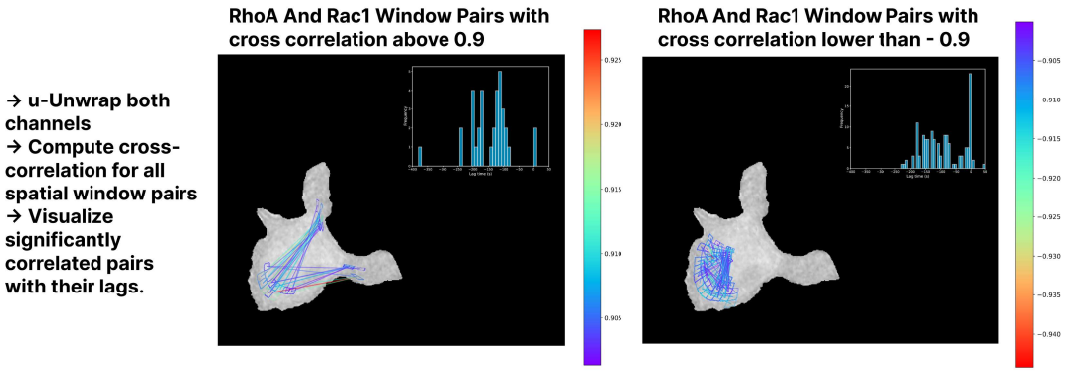

Fig. S4: Long range correlation pairs detectable with the help of u-Unwrap pipeline

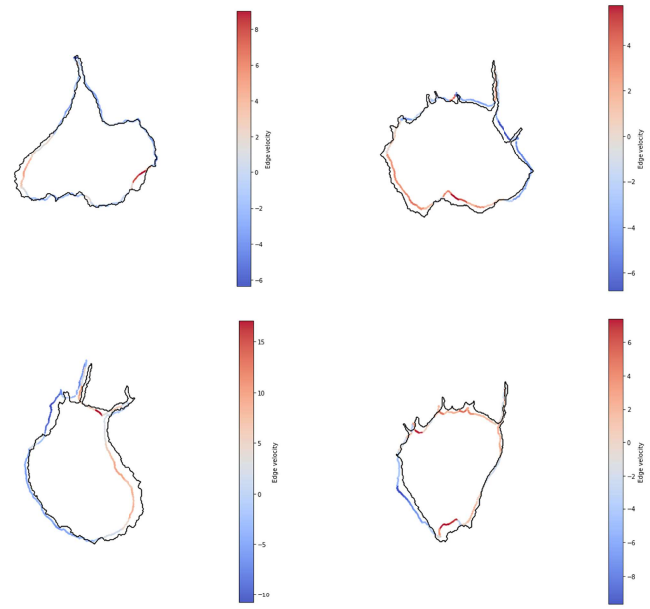

Edge velocity visualization:
Red indicates positive values, blue indicates negative values.
Black lines show the contour in the next frame.

Fig. S5: Edge Velocity Calculation